BUTTERWORTH HEINEMANN

Polymer Vol. 36 No. 12, pp. 2331–2341, 1995

0032-3861/95/$10.00 + 0.00

Morphological characterization of injection moulded syndiotactic polystyrene

Leonardo C. López*, Robert C. Cieslinski, Curt L. Putzig and Rosemarie D. Wesson†

The Dow Chemical Company, Midland, MI 48674, USA
(Received 30 April 1993; revised 16 November 1994)

The morphology of syndiotactic polystyrene (s-PS) injection moulded at 50°C and 160°C was examined using polarized optical microscopy, transmission electron microscopy, and Fourier transform infra-red microspectroscopy as a function of mould temperature. A skin/core effect was present and significant structural differences existed at the skin of samples moulded at these two temperatures. Bars moulded at 50°C presented a 'shish kebab' morphology at the surface while samples moulded at 160°C had 'sheaf' structures. In the sample moulded at 50°C, crystallinity increased from 19% at the surface to 41% at depths $>250\,\mu$m. Such a gradient was not present in the sample moulded at 160°C, which had 46% crystallinity throughout. This crystallinity gradient in samples moulded at 50°C was responsible for the lower chemical resistance of such samples.

(Keywords: syndiotactic polystyrene; morphology; crystallinity)

INTRODUCTION

Syndiotactic polystyrene (s-PS) has the characteristics to be a technologically important thermoplastic. In the last few years, significant effort has been placed on studying the processing and crystallization behaviour of s-PS. During these studies it was observed that, although a mould temperature of 50°C allows faster production of parts than a mould temperature of 160°C, there were significant differences in the macroscopic morphology and properties of the injected samples. In particular, differences in the chemical resistance of the polymer were recorded. For example, samples moulded at 160°C had higher resistance to organic solvents than samples moulded at 50°C. Consequently, the microscopic crystalline structure of samples injection moulded at these temperatures was studied to determine whether crystallinity content or superstructure was the contributing factor to the different behaviours.

Although isotactic polystyrene (i-PS) has been known since 1955, it was only in recent years that syndiotactic polystyrene was synthesized with high stereoregularity[1,2]. The high melting point ($\approx$275°C), crystallinity and chemical stability of syndiotactic polystyrene are some of the interesting properties that have brought considerable attention to it. In addition, its crystallization rate as measured by spherulitic growth is more than an order of magnitude higher than that of i-PS at the same supercooling[3]. Therefore, s-PS presents characteristics that make it a technologically important polymer.

Syndiotactic polystyrene has a very complex polymorphic behaviour that has been the subject of many publications. Most studies have focused on characterization of the various crystalline unit cell structures, chain conformations and their relationship to crystallization conditions by X-ray diffraction[4–11], by Fourier transform infra-red spectroscopy[12–18], by solid-state nuclear magnetic resonance spectroscopy[1,19,20] and by electron diffraction[21,22]. Several crystalline forms have been identified. For instance, crystallization from the melt can produce two crystalline species that contain planar zig-zag chains, with an identity period $c=5.1$ Å. The α-form has a hexagonal unit cell with dimension $a=26.3$ Å (refs 9, 21), whereas the β-form is orthorhombic with $a=8.81$ Å and $b=28.82$ Å (ref. 11). Moreover, solvents like methylene chloride induce a crystalline form with helical chain conformation[4,5,7,8,20,23,24]. Glassy s-PS films and films crystallized in the α-form treated with methylene chloride originate a δ-form with 2_1 helical conformation having an identity period of 7.5 Å. This crystalline form includes solvent molecules in the structure[4,7,8,20,23,25]. Other solvents produce the same effects. Upon complete desiccation, the δ-form transforms into yet another crystalline species (γ), also with helical chain conformation[8,23]. Under the injection moulding conditions utilized in this study, the α-form is obtained.

EXPERIMENTAL

Syndiotactic polystyrene with weight-average molecular weight of 418 000 g mol^{-1} and polydispersity ratio of 2 after extrusion was utilized. The level of syndiotacticity was >95%. In this study, injection moulded dogbone tensile bars (3 mm thickness) were produced at mould temperatures of 50°C and 160°C. The injection velocity

* To whom correspondence should be addressed
† Current address: Battelle 505 King Ave., Columbus, OH 43201, USA

and holding pressure were maintained constant. The cycle time was essentially doubled at the high mould temperature. The melt temperature was 320°C. Under these melting and moulding conditions, the α crystalline form is obtained[8].

The crystalline superstructures were examined by polarized optical microscopy. Sections approximately 2 μm thick were microtomed to perform the optical microscopy analysis. A Zeiss Axiomat microscope in the polarized transmission geometry was utilized. Transmission electron microscopy (TEM) was performed to study the lamellar level structure using a Hitachi H600 transmission electron microscope.

Sample preparation for TEM studies was more involved because the small electron density difference between the crystalline and amorphous phases precluded their differentiation by conventional TEM. Therefore, methods to increase the electron density difference needed to be implemented. This can be accomplished by conducting a chemical reaction in such conditions that the chemical reacts at a faster rate or exclusively with the amorphous phase, leading to the deposition of a high electron density reactant in the amorphous phase. Various etching and staining procedures were evaluated: chlorosulfonation with chlorosulfonic acid and post-treatment with a 1% aqueous solution of uranyl acetate; etching with potassium permanganate in sulfuric acid; etching with concentrated nitric acid; and staining with ruthenium tetraoxide. This latter staining method was found to be the most effective method for increasing the contrast.

Staining was performed with both commercial and fresh ruthenium tetraoxide. The latter was prepared by reaction of ruthenium trichloride hydrate with 5 ml of 5.5% sodium hypochlorite aqueous solution at room temperature[25]. Pieces of s-PS were stained with the RuO_4 solution prior to microtoming the 800–1000 Å thick sections. In addition, fresh thin sections, 800–1000 Å thick, were stained by exposure to RuO_4 vapour.

Due to the morphological anisotropy that can be expected in injection moulded parts, characterization of these samples needs to be performed in at least two perpendicular directions. The directions are defined as the microtoming direction in relation to the main component of the flow. *Figure 1* shows schematically the observation directions. The parallel and perpendicular sections were obtained from the centre of the bar to minimize the effects from side boundary layers. The flat cut sections were prepared by sectioning layers of the sample starting at the surface and continuing inwards through the thickness of the sample.

The crystallinity of the injection moulded samples was determined by Fourier transform infra-red (*FT*i.r.) microspectroscopy. A Nicolet 60SX FT-IR fitted with a Digilab i.r. microscope attachment and a SpectraTech motorized micropositioning stage was used. This motorized micropositioning stage allowed the collection of i.r. spectra from small areas (20 μm in diameter). Syndiotactic polystyrene sections approximately 10 μm thick were microtomed for the *FT*i.r. analysis. A Reichert Ultracut E ultramicrotome was utilized for all the sectioning.

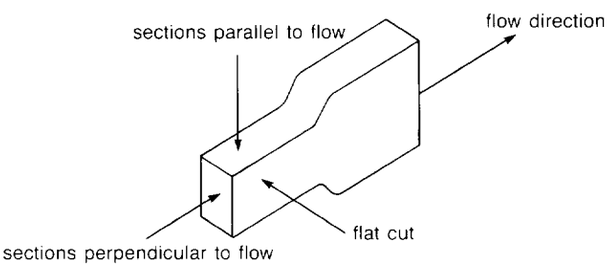

Figure 1 Tensile bar schematic defining the observation directions in relation to the main flow component

RESULTS

Optical microscopy

Figures 2 and *3* present optical micrographs corresponding to samples moulded at 50 and 160°C, respectively. In each figure, cross-sections of the tensile bars parallel and perpendicular to flow are shown. Clearly, these micrographs exhibit a morphology variation within the bar cross-section. It is important to note that the sections are birefringent in all the areas, indicating that there is crystallinity within the whole cross-section of the tensile bars.

A detailed analysis of the sections parallel to flow shows five areas of different birefringence intensity. The samples moulded at 50°C present a highly birefringent area that

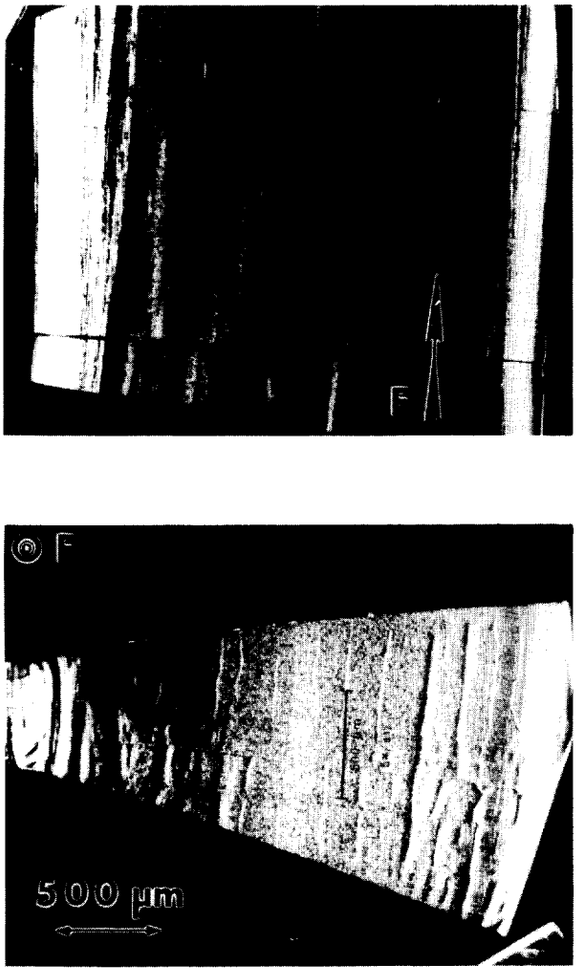

Figure 2 Polarized optical micrographs of cross-sections of injection moulded tensile bars. Mould temperature: 50°C. The arrow and dot show the flow direction

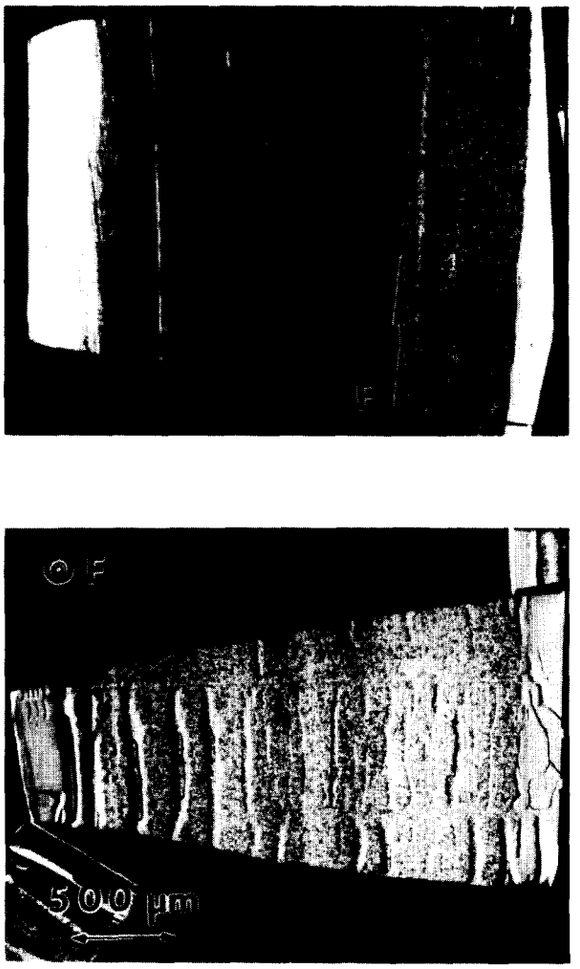

Figure 3 Polarized optical micrographs of cross-sections of injection moulded tensile bars. Mould temperature: 160°C. The arrow and dot show the flow direction

extends for ~200 μm from the surface of the bar. This skin, which appears as transparent in the tensile bars, has been previously assumed amorphous. However, the high birefringence reveals that the skin is oriented and/or crystalline.

Following the skin, there is a 150 μm thick shear zone characterized by the presence of a blend of spherulitic and row nucleated species, with the rows oriented parallel to the direction of flow. This region will be referred to as the intermediate area. Further into the thickness, the 1900 μm thick core seems to be spherulitic. However, the spherulite size is too small to be characterized by optical microscopy. Continuing across the section, another intermediate region appears, followed by the other skin.

The samples moulded at 160°C present essentially the same five areas. Nevertheless, the zone thicknesses are different. The skin is 250 μm thick and highly birefringent. The shear zone (90 μm thick) is thinner than that of the cold mould samples (150 μm). The core is spherulitic and extends for ~2300 μm.

Observation of the sections cut perpendicular to flow only allowed discerning between the skin and core of both cold and hot mould samples. The intermediate regions are not noticeable because they present birefringent patterns similar to those of spherulites.

Transmission electron microscopy

Staining of thin sections with RuO_4 vapour was found to be the best etching and staining method. *Figure 4* shows a TEM micrograph of an s-PS section stained with RuO_4 vapour. The spherulitic texture presents very good detail. Furthermore, the lamellar crystals are very well resolved. These are represented by the lighter bands whereas the interlamellar material is dark due to deposition of ruthenium. The staining time was approximately 4 minutes. A study of the effect of section thickness on the staining routine indicated that sections 800–1000 Å thick provide the best contrast. For future reference, it is worth describing an artefact present in this micrograph. The randomly distributed dark spots in this micrograph are deposits of excess RuO_4 on the film. The amount of precipitates seemed to be related to the concentration of residuals in s-PS. This artefact will be present in some of the micrographs. Notwithstanding, the deposits do not interfere with the morphological observations.

Samples moulded at 160°C

Figure 5 shows sections of samples moulded at 160°C and microtomed parallel to flow (defined in *Figure 1*). As indicated by optical microscopy, the core is spherulitic. However, the spherulites are not fully developed: they are 'sheaf structures'. These sheaf structures have an elliptical profile (7 × 5 μm) with the short radius oriented parallel to flow. The presence of sheaf structures indicates that there is a low strain induced in the core of the tensile bars through injection moulding, thus allowing for a close to quiescent crystallization. The formation of sheaf

Figure 4 Transmission electron micrograph of injection moulded s-PS. Thin sections stained with ruthenium tetraoxide vapour

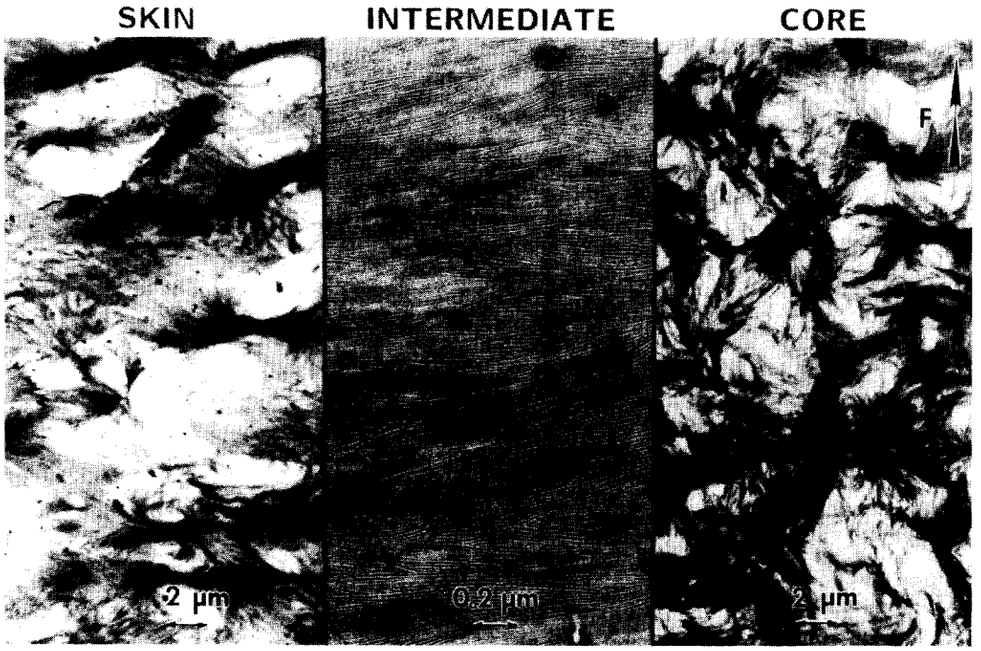

Figure 5 Transmission electron micrographs of a sample injection moulded at 160°C. Sections were microtomed parallel to flow

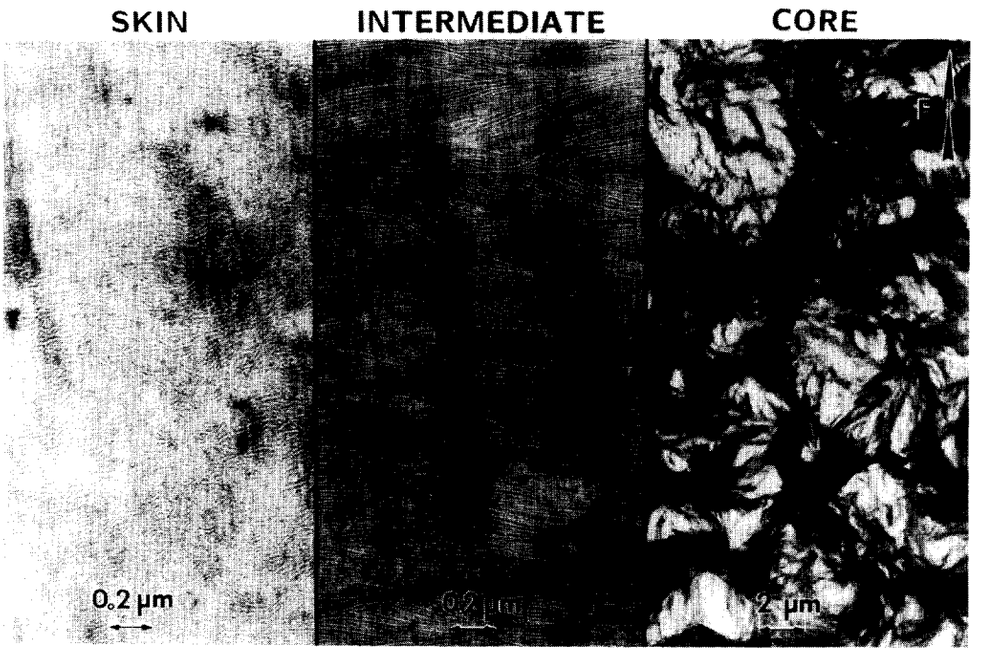

Figure 6 Transmission electron micrographs of a sample injection moulded at 160°C. Flat cut sections

structures is due not only to the small orientation effect that may be present, but also to the high crystallization rate of s-PS at the moulding temperature. It has been reported that the spherulitic growth rate of s-PS is an order of magnitude higher than that of i-PS under the same supercooling conditions[3]. Nevertheless, quiescent crystallization at higher temperatures (260°C) has yielded fully developed spherulites[3]. Higher magnification observation of the sheaf structures indicated a lamellar thickness of 140 Å.

The intermediate region starts at 40 μm from the surface of the specimen and extends to $\sim$250 μm. This region comprises lamellar crystals oriented perpendicular to the direction of flow. The superstructure consists of a 'shish kebab' species with a high concentration of lamellar crystals. Shish kebab morphology is formed under higher strain conditions than sheaf structures; therefore, there is more polymer chain orientation in the intermediate area. Assuming that the long chain axis is perpendicular to the lamellar length in the crystals, one can infer that polymer chain orientation is parallel to flow in this area. Electron diffraction data support this statement. The lamellar thickness is 80 Å in this region.

The skin of samples moulded at 160°C is composed of

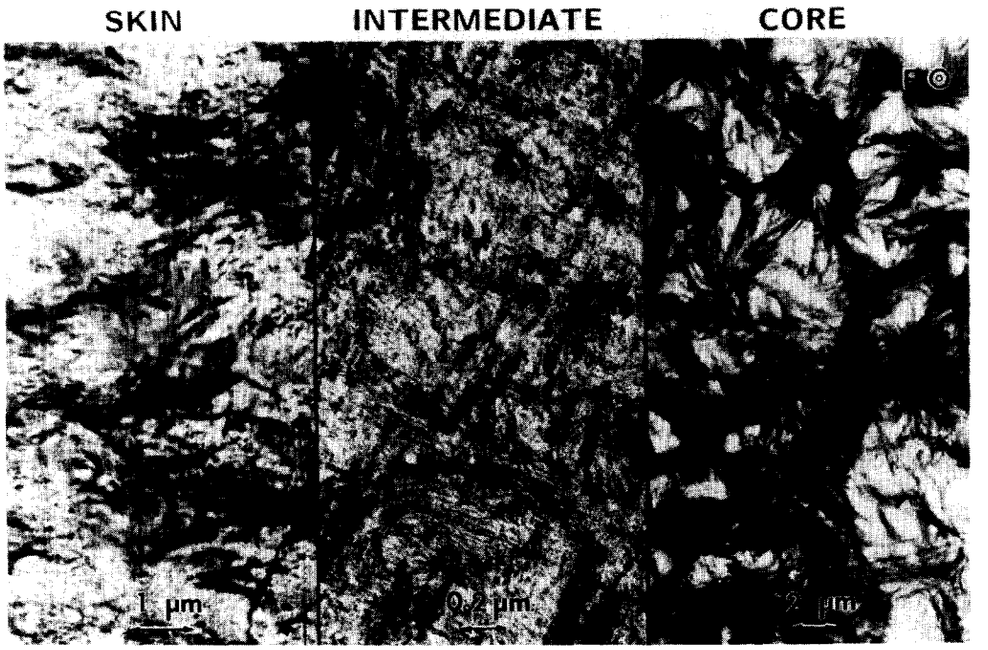

Figure 7 Transmission electron micrographs of a sample injection moulded at 160°C. Sections were microtomed perpendicular to flow

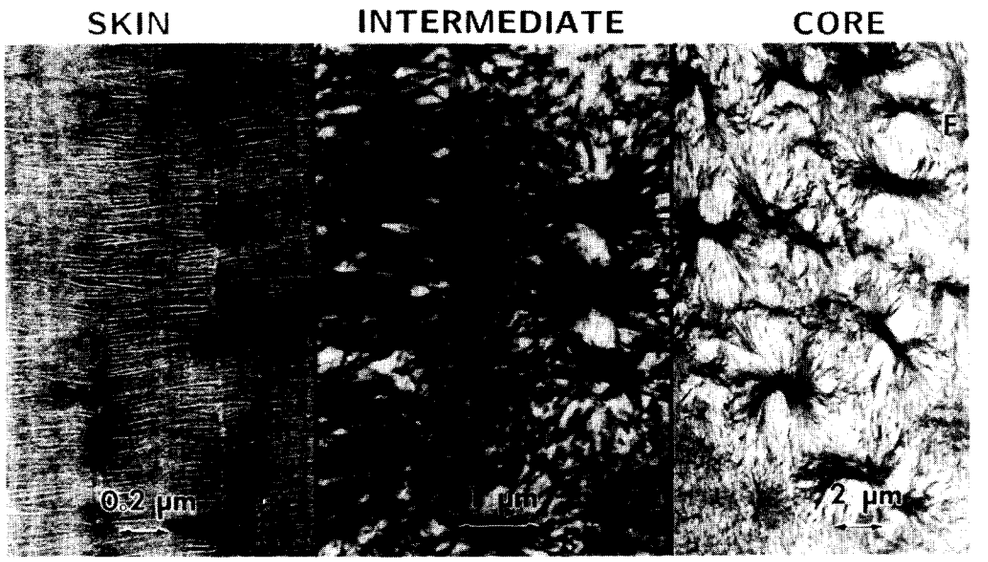

Figure 8 Transmission electron micrographs of a sample injection moulded at 50°C. Sections were microtomed parallel to flow

4×6 μm sheaf structures. The lamellar thickness is 80 Å in this area. *Figure 6* presents micrographs of flat cut sections corresponding to a hot mould sample. Because this direction of observation is equivalent to that of the sections parallel to flow, the same type of morphology is observed at the core and intermediate regions. The skin, however, shows short lamellar crystals that are randomly oriented, resembling the tips of the sheaf structures. Since this section is the surface of the bar, the observed morphology indicates that the sheaf structures do not nucleate at the surface of the mould but rather at a certain distance beneath.

Figure 7 shows sections microtomed normal to the flow. These sections present sheaf structures in the core and skin. The intermediate region, however, has a rough texture with some randomly oriented lamellar crystals. In these sections, the direction of observation is along the flow; therefore, in the intermediate area, the tips of the shish kebab structures are found. The rough texture is due to the fact that the lamellar planes are parallel to the plane of the micrograph. The appearance of some randomly oriented lamellae may be due to folding or misorientation of the lamellar crystals at the outer boundaries of the shish kebab.

Samples moulded at 50°C

Figure 8 shows sections of samples moulded at 50°C that were microtomed parallel to flow. The core exhibits 4×6 μm sheaf structures with rougher texture than those observed in the core of the hot mould sample. This may be due to the faster cooling rate that the cold mould samples experience. The sheaf size is very similar in cold

and hot mould samples indicating that the nucleation density at the core is approximately the same regardless of the mould temperature. The lamellar thickness at the core is 100 Å.

The intermediate region, spanning for 150 μm, is composed of a mixture of sheaf structures, row nucleated species and shish kebabs. This is a zone between the core and the skin in which the flow pattern is in transition from the very low shear front in the core of the sample, increasing gradually to high shear as the mould surface is approached. Therefore, the degree of chain orientation in this region would increase in the same order. As a consequence, the sheaf structures evolve to row nucleated species and to shish kebabs. For instance, in this region, sheaf structures are smaller and nucleate closer to each other than in the core. In particular, their dimension in the flow direction becomes smaller and the sheaf characteristics are lost in row structures and shish kebabs. However, a lamellar thickness of 80 Å is maintained in both structures, sheaf and shish kebab, in this intermediate region.

The skin presents well-defined shish kebab morphology with chain orientation parallel to the direction of flow. The lamellar crystals composing the shish kebabs interleave very well with neighbouring shish kebabs. Furthermore, there seems to be a high shish content. The shish kebab crystals can be easily seen in the picture and are separated by < 1 μm. The lamellar thickness in this area is 70 Å.

In flat cut sections, the direction of observation presents the same morphological perspective as the sections cut parallel to flow. The skin, however, exhibits shish kebabs which are short with narrow dimensions and lamellar thickness of 130 Å (*Figure 9*). Since the polymer chains are oriented in the direction of flow, the thicker lamellae suggest a higher effective elongational flow in this region. This is in contrast to the observations at the skin of the hot mould sample that presented sheaf structures. Another interesting observation is the fact that the shish kebabs are separated, implying that crystallinity at the surface of the cold mould samples is lower than that at the core.

In sections microtomed normal to flow, the core shows the usual sheaf structures (*Figure 10*). The intermediate area has some sheaf structures and circular rough species that represent the shish kebab and row structure tips. The skin also exhibits this circular rough species with lamellar crystals on the outskirts that seem oriented radially. The central rough area would be the plane of the lamellar crystals that constitute the shish kebabs whereas the lamellae at the outskirts would be due to folding or misorientation at the ends of the lamellar crystals.

Fourier transform infra-red spectroscopy

In the previous section, there were indications of a lower crystallinity in the skin of samples moulded at low temperature. Consequently, direct measurements of crystallinity were carried out at the skin and core of the injection moulded samples. Crystallinity measurements can be performed by wide angle X-ray scattering techniques, differential scanning calorimetry, density gradient column and *FT*i.r. Calorimetric techniques and density gradient column represent a problem in the study of thin films due to the large sample size required. The wide angle X-ray scattering technique was not successful for thin films of s-PS because the diffraction peaks are not very well defined at low crystallinities. In addition, gas scattering produced a higher amorphous contribution that interfered further with the measurements.

*FT*i.r. is the technique of choice if bands corresponding to vibrations in the crystalline state can be identified. *Figure 11* shows the 1250–1420 cm^{-1} area of the *FT*i.r. spectra for bulk s-PS samples having different degrees of crystallinity. The intensity of the 1333 cm^{-1} band decreases as crystallinity decreases; therefore, it can be

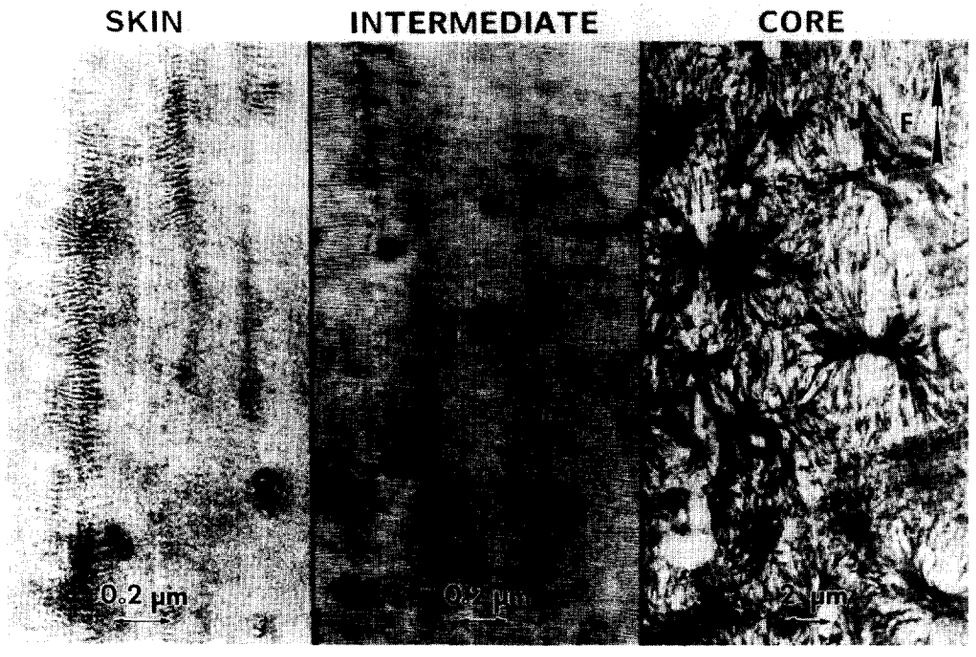

Figure 9 Transmission electron micrographs of a sample injection moulded at 50°C. Flat cut sections

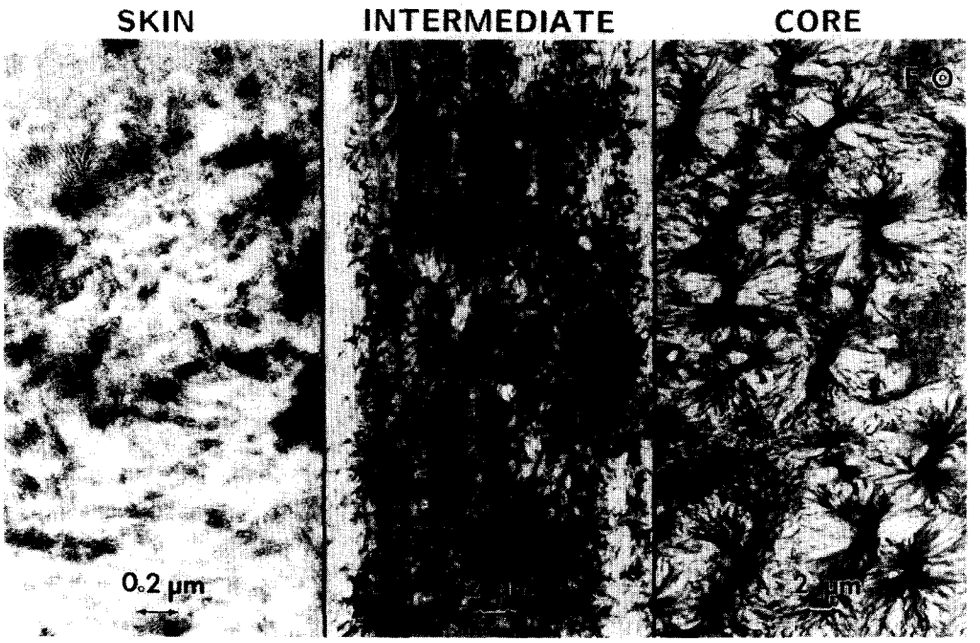

Figure 10 Transmission electron micrographs of a sample injection moulded at 50°C. Sections were microtomed perpendicular to flow

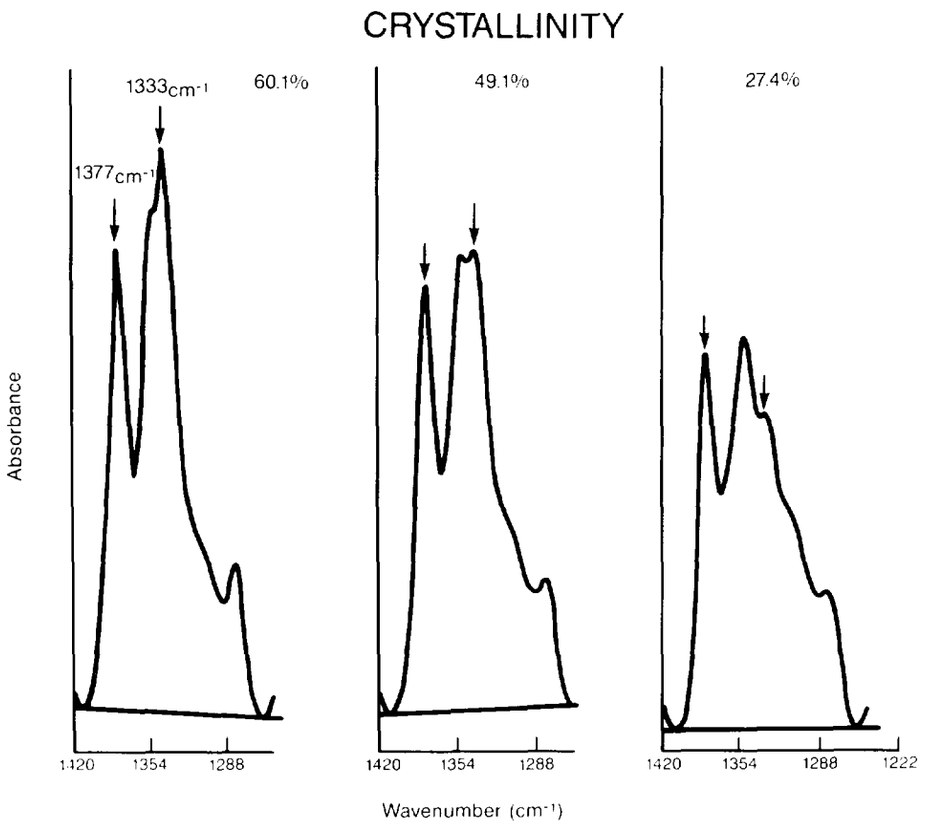

Figure 11 *FT*i.r. spectra in the 1250–1420 cm^{-1} range corresponding to s-PS specimens with various degrees of crystallinity. Note bands at 1333 and 1377 cm^{-1} marked by arrows

associated with vibrations occurring in the crystalline phase. Furthermore, the intensity of the 1377 cm^{-1} band remains approximately constant as the crystallinity varies. The ratio of the intensity of these two bands was used to approximate crystallinity. *Figure 12* shows a plot of the ratio of intensity of the 1333 cm^{-1} band to that of the 1377 cm^{-1} band as a function of crystallinity determined by differential scanning calorimetry (d.s.c.). There is a linear relationship between the |1333|/|1377| ratio and crystallinity by d.s.c. as follows:

$$|1333|/|1377| = 0.0141X + 0.3025 \quad (1)$$

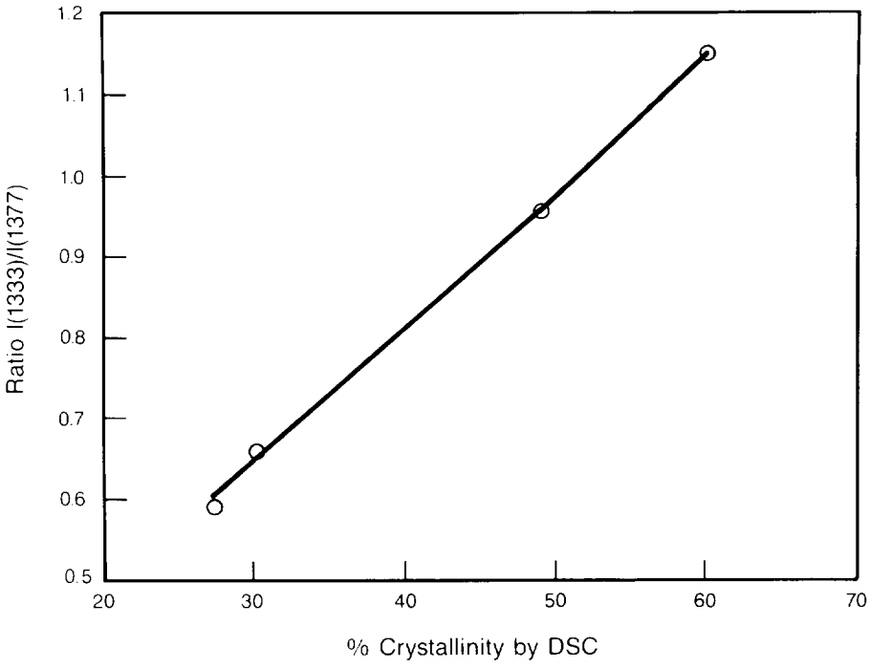

Figure 12 Relationship between the ratio of intensities of bands at 1333 and 1377 cm^{-1} (|1333|/|1377|) and per cent crystallinity determined by d.s.c.

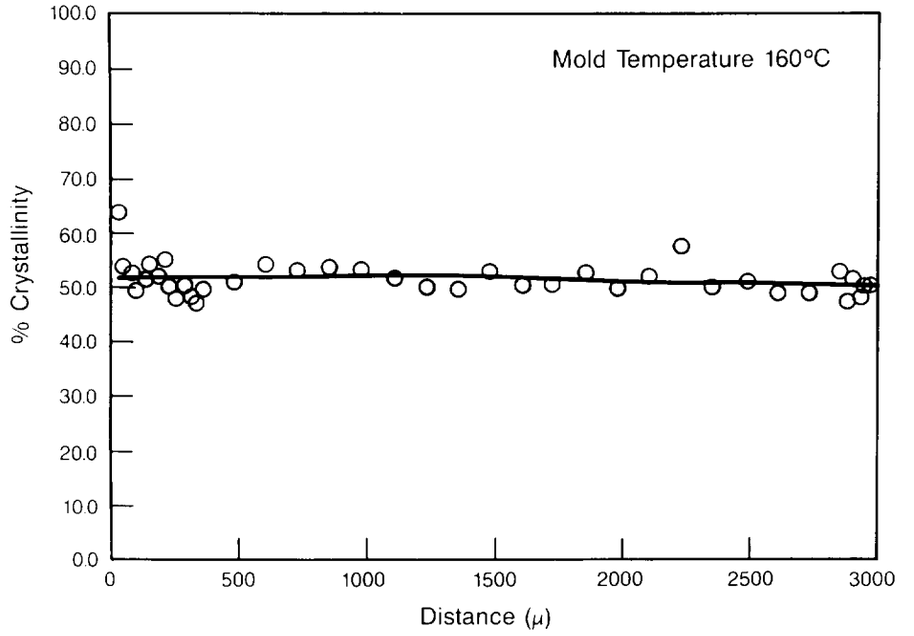

Figure 13 Graph of crystalline content as a function of position corresponding to samples moulded at 160°C. In the graph, 0 and 3000 μm represent the surfaces of the injection moulded samples

where X is per cent crystallinity determined by d.s.c. This linear relationship was used to estimate semiquantitatively the crystallinity of s-PS microtomed thin sections by *FT*i.r.

Measurement on samples moulded at 160°C showed similar crystallinities at the core and skin (46% and 42%, respectively). Samples moulded at 50°C, however, exhibited 19% crystallinity at the surface, whereas at the core it was 41%. Utilizing an *FT*i.r. microspectrometer, the crystallinity profile as a function of distance from the mould surface was measured in samples moulded at 160°C and 50°C. *Figures 13* and *14* present plots of crystalline content as a function of distance from the mould surface for samples moulded at 160 and 50°C, respectively. In samples moulded at 160°C, the crystalline content remains constant at ~50% throughout the thickness of the bar. On the other hand, samples moulded at 50°C have a lower crystallinity value at the two surfaces. In the core, the crystalline content is ~50% whereas at the surface it decreases to 20%. This decrease in crystallinity occurs within 200 μm from the surface, which coincides with the skin thickness observed by

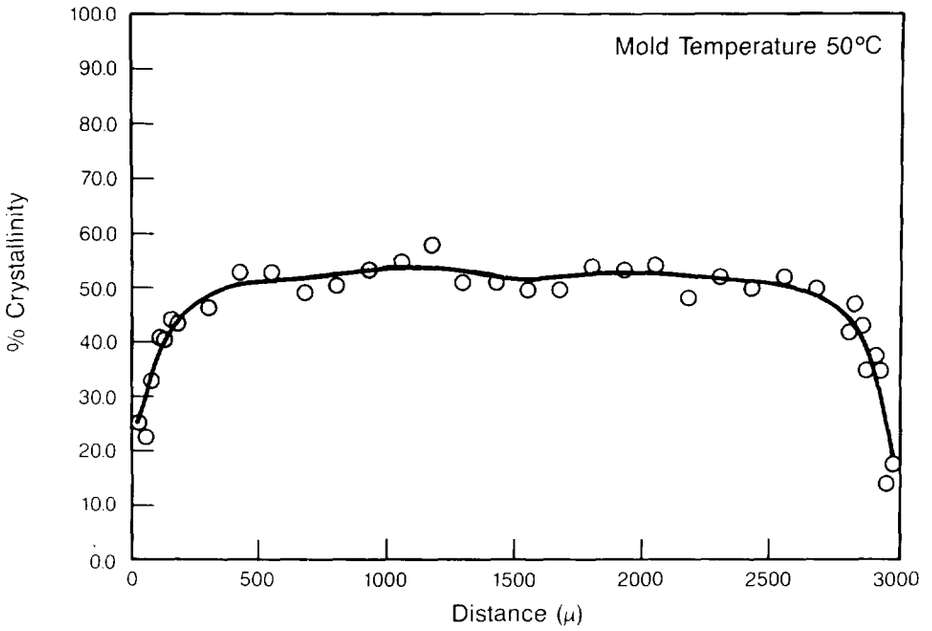

Figure 14 Graph of crystalline content as a function of position corresponding to samples moulded at 50°C. In the graph, 0 and 3000 μm represent the surfaces of the injection moulded samples

optical microscopy. Moreover, indications of lower surface crystalline content in samples moulded at 50°C were also observed in the microscopy study. Specifically, in flat cut sections (*Figure 9*) the skin presented very short shish kebabs with narrow dimensions and separated by featureless material. Since the crystallinity values were slightly higher when determined by *FT*i.r. microspectrometry, the effects of birefringence on these *FT*i.r. measurements were analysed by changing polarization during the measurements. The same results were found, establishing the validity of our experimental findings.

DISCUSSION

Samples moulded at 50°C had high orientation structures such as shish kebab structures at the skin. The highly oriented superstructures decreased as the core of the sample was approached. These are the expected results for moulding with cold moulds. The orientation close to the mould wall would be the result of fountain type of flow in the advancing front[26]. The resulting oriented polymer layer crystallizes upon contact with the cold mould wall, retaining the orientation. Therefore, the crystallization process produces a highly oriented morphology (shish kebabs). Below the surface, the molecular orientation obtained in the moulded article would be resulting from a fully developed shear flow behind the front. The final orientation distribution in the moulded piece is dependent on the cooling rate, the spectrum of relaxation times and the kinetics of crystallization. As expressed earlier, the crystallization rates of s-PS are rather fast. Therefore, at low mould temperatures crystallization takes place quickly upon contact with the cold wall, maintaining the orientation. In samples moulded at 160°C, the skin morphology was different. In this case, sheaf structures nucleated slightly below the surface were observed. This indicates that crystallization occurred from a melt with very low orientation and that nucleation was not heterogeneously induced by the mould wall. This may result from short relaxation times and relatively long nucleation induction times at the high mould temperature utilized. However, below the surface, the superstructure in the intermediate area (below the skin) presents shish kebab morphology, which indicates that orientation prevailed in this region.

The skin–core morphology behaviour of s-PS injection moulded at 50°C has been observed in other injection moulded polymers. For example, Clark[27] and Boehme[28] reported that injection moulded acetal homopolymers can have laminate structure under certain moulding conditions. In those publications, the mouldings had a skin with high molecular orientation, similar to shish kebab structures, an intermediate region with lower orientation that they termed 'transcrystalline layer' and a spherulitic core. Saiu *et al.*[29] reported similar findings on injection moulded isotactic polypropylene (i-PP), having an isotropic spherulitic core, a crystalline skin layer and an intermediate layer with cylindritic type crystallization growth from strained nuclei. This intermediate layer had the lamellar stacks with the *b*-axis oriented along the flow direction. Wenig and Herzog[30] also described the morphology of injection moulded i-PP as having an unoriented spherulitic core and an oriented shish kebab type structure in samples moulded at 60, 80 and 120°C. These descriptions are similar to those found in our study of s-PS when moulded at 50°C, where three regions of morphology can be identified. However, in our findings, the core morphology has some degree of orientation as can be discerned from the sheaf structures. Furthermore, the intermediate region in s-PS is a transitional zone where the superstructure varies from sheaf to row nucleated and to shish kebab structures, suggesting an intermediate degree of orientation. The skin morphology of s-PS samples moulded at 160°C was also different, presenting sheaf structures, indicative of low orientation. Another difference in our observations was the variation of the lamellar thickness with distance from the surface of the samples. For s-PS, under the conditions

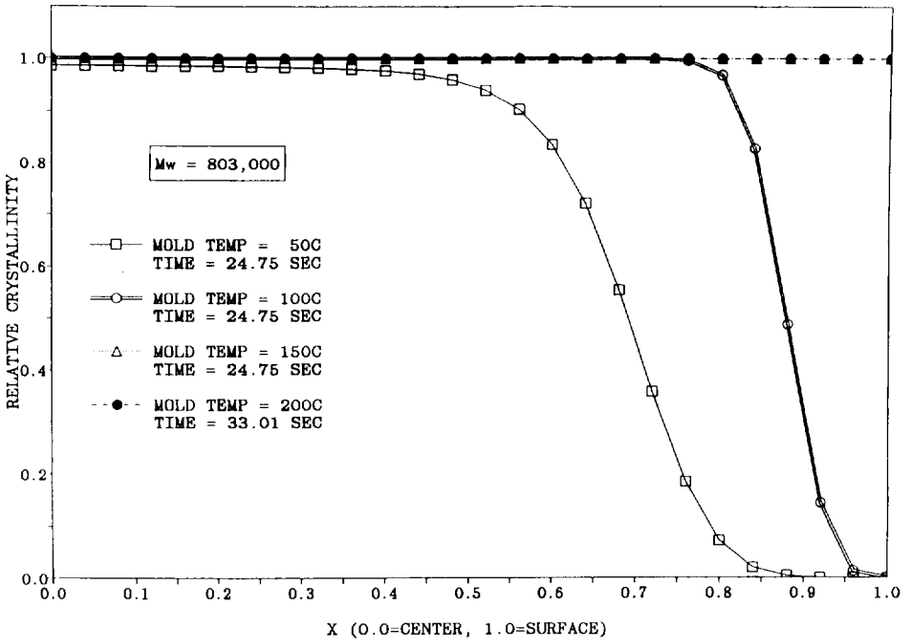

Figure 15 Final crystallinity profiles for the solidification of syndiotactic polystyrene at various mould temperatures (from ref. 34)

used here, the lamellar thickness increases as distance from the surface increases. In contrast, Wenig and Herzog[30] reported that lamellar thickness in the skin layer of i-PP was higher than that in the core.

The crystallinity profiles of s-PS samples moulded at 50°C indicated a decrease from 41% at the core to 19% at the skin. Similar decreases in crystallinity as the surface of the moulded article is approached have been reported for other polymers such as i-PP[29,30], polyethylene[31], nylon-6[32] and poly(tetramethylene terephthalate)[33]. The s-PS samples moulded at 160°C, however, did not show such a variation of crystallinity as a function of distance from the surface of the sample. The crystalline profile in a moulded s-PS sample has been analysed by Wesson[34]. In this analysis, Wesson utilized a one-dimensional heat transfer model to simulate the cooling of an s-PS sample from the melt at 300°C in contact with a mould at lower temperature. Incorporating crystallization kinetic data of s-PS and using finite-difference approximations, the crystallinity profile as a function of distance from the centre of the samples was calculated for various mould temperatures. These calculations predicted that for mould temperatures higher than 150°C, the relative crystalline content was constant throughout the sample thickness. On the other hand, lower mould temperatures produced a crystallinity gradient from the sample core to a completely amorphous surface (*Figure 15*). Our experimental findings also showed lower crystallinity at the surface of samples crystallized in moulds at 50°C. However, the skin had crystalline content of 20%. This discrepancy is due to the fact that the calculations made by Wesson[34] did not include contributions from elongational and shear fields to induction of crystallinity at the surface of the cooling samples. This is an important consideration in view of the shish kebab morphology observed at the skin of samples injected into moulds at 50°C (*Figures 8* and *9*). Consequently, this contribution would have to be incorporated into the model to acquire a more accurate analysis.

Table 1 Lamellar crystallite thickness (Å) for samples injection moulded at different mould temperatures

	Mould temperature (°C)	
	50	160
Skin parallel to flow	70	80
Intermediate parallel to flow	80	80
Core parallel to flow	100	140

In terms of the effect of morphology on the chemical resistance of s-PS, there are several structural parameters that need consideration. Our experimental evidence indicates crystallinity and/or orientation as probable important variables affecting solvent resistance. Crystallite size does not seem to play a significant role. For instance, *Table 1* shows the lamellar crystallite thickness in bars injection moulded at 50 and 160°C obtained from measurements on TEM micrographs. At the surface and intermediate regions, the cold and hot mould bars have the same lamellar size. In other words, the different chemical resistance of these samples is not due to different crystallite size. Superstructure may be another contributing factor to produce different chemical resistance. The superstructure was different at the skin of the moulded samples. For instance, samples moulded at 50°C presented shish kebab structures at the skin whereas samples moulded at 160°C had sheaf structures. This is the direct consequence of higher levels of orientation at the skin of samples moulded at 50°C. However, crystalline content is a far more important factor. The data in *Figures 13* and *14* clearly show that samples moulded at 50°C had crystallinity at the skin reduced by 50% from that of the core. This did not occur in samples moulded at 160°C. Furthermore, since the core crystallinity is the same in cold and hot mould samples, the surface crystalline content should be critical in defining the solvent resistance of the injection moulded s-PS parts. In fact, the effects of lower surface crystalline

content on solvent resistance of s-PS has been reported recently[35]. Malanga and Newman[35] clearly showed that samples with low surface crystallinity had higher benzene adsorption. The weight gain of the s-PS samples exposed to benzene decreased as the surface crystalline content increased.

CONCLUSIONS

The study of the morphological textures of injection moulded s-PS revealed a skin/core morphology gradient. Major structural differences were observed at the skin of samples moulded at 50 and 160°C. Tensile bars moulded at 50°C presented shish kebab structures at the surface while samples moulded at 160°C had sheaf morphology. Moreover, there was a gradient of crystallinity at the surface of samples moulded at 50°C, the crystallinity varying from 19% at the surface to 41% in the core. This variation occurred within 250 μm of the surface. The samples moulded at 160°C presented crystallinity of 46% over their entire thickness. The lower crystallinity of samples moulded at 50°C is a major factor producing the lower chemical resistance of s-PS bars previously reported[35].

ACKNOWLEDGEMENTS

The authors express their sincere gratitude to D. W. Susnitzky, B. G. Landes and D. Krueger for providing valuable data and discussions, and A. E. Platt for his continued support throughout the project.

REFERENCES

1 Ishihara, N., Seimiya, T., Kuramoto, N. and Uoi, M. *Macromolecules* 1987, **19**, 2464
2 Pellecchia, C., Longo, P., Grassi, A., Ammendola, P. and Zambelli, A. *Makromol. Chem., Rapid Commun.* 1987, **8**, 277
3 Cimmino, S., Di Pace, E., Martuscelli, E. and Silvestre, C. *Polymer* 1991, **32**, 1080
4 Immirzi, A., De Candia, F., Ianelli, P., Vittoria, V. and Zambelli, A. *Makromol. Chem., Rapid Commun.* 1988, **9**, 761
5 Vittoria, V., Russo, R. and De Candia, F. *J. Macromol. Sci.-Phys.* 1989, **B28**, 419
6 Vittoria, V., Russo, R. and De Candia, F. *Makromol. Chem., Macromol. Symp.* 1990, **39**, 317
7 Vittoria, V., Ruvolo Filho, A. and De Candia, F. *Polym. Bull.* 1991, **26**, 445
8 Guerra, G., Vitagliano, V. M., De Rosa, C., Petraccone, V. and Corradini, P. *Macromolecules* 1990, **23**, 1539
9 De Rosa, C., Guerra, G., Petraccone, V. and Corradini, P. *Polym. J.* 1991, **23**, 1435
10 Guerra, G., De Rosa, C., Vitagliano, V. M., Petraccone, V. and Corradini, P. *J. Polym. Sci., Polym. Phys. Edn* 1991, **29**, 265
11 De Rosa, C., Rapaccioulo, M., Guerra, G., Petraccone, V. and Corradini, P. *Polymer* 1992, **33**, 1423
12 Nyquist, R. A. *Appl. Spectrosc.* 1989, **43**, 440
13 Guerra, G., Musto, P., Karasz, F. E. and McKnight, W. J. *Makromol. Chem.* 1990, **191**, 2111
14 Ruvolo Filho, A. and Vittoria, V. *Makromol. Chem., Rapid Commun.* 1990, **11**, 199
15 De Candia, F., Ruvolo Filho, A. and Vittoria, V. *Colloid Polym. Sci.* 1991, **269**, 650
16 De Candia, F., Ruvolo Filho, A. and Vittoria, V. *Makromol. Chem., Rapid Commun.* 1991, **12**, 295
17 Vittoria, V. *Polym. Commun.* 1990, **31**, 263
18 Reynolds, N. M. and Hsu, S. L. *Macromolecules* 1990, **23**, 3463
19 Grassi, A., Longo, P. and Guerra, G. *Makromol. Chem., Rapid Commun.* 1989, **10**, 687
20 Gomez, M. A. and Tonelli, A. E. *Macromolecules* 1990, **23**, 3384
21 Greis, O., Xu, Y., Asano, T. and Petermann, J. *Polymer* 1989, **30**, 591
22 Pradère, P. and Thomas, E. L. *Macromolecules* 1990, **23**, 4954
23 Vittoria, V., Russo, R. and De Candia, F. *Polymer* 1991, **32**, 3371
24 Montezinos, D., Wells, B. G. and Burns, J. L. *J. Polym. Sci., Polym. Lett. Edn* 1985, **23**, 421
25 Vittoria, V., Ruvolo Filho, A. and De Candia, F. *J. Macromol. Sci.-Phys.* 1991, **B30**, 155
26 Tadmor, Z. and Gogos, C. 'Principles of Polymer Processing', J. Wiley and Sons, Inc., New York, 1979
27 Clark, E. S. *Polym. Prepr.* 1973, **14**, 268
28 Boehme, E. *Kunststoffe* 1970, **60**, 273
29 Saiu, M., Bracto, V., Piccarolo, S. and Titomanlio, G. *Int. Polym. Process.* 1992, **7** (3), 267
30 Wenig, W. and Herzog, F. *J. Appl. Polym. Sci.* 1993, **50**, 2163
31 May, F. H. and Kamal, M. R. *Polym. Eng. Sci.* 1980, **20** (14), 957
32 Russel, D. P. and Beaumont, P. W. *J. Mater. Sci.* 1980, **15**, 197
33 Callear, J. E. and Shortall, J. B. *J. Mater. Sci.* 1977, **12**, 141
34 Wesson, R. D. SPE Tech. Papers, SPE ANTEC Meeting, May 1990, Dallas, TX, pp. 574–590
35 Malanga, M. T. and Newman, T. H. Fourth SPSJ Int. Polym. Conf., November 1992, Yokohama, Japan